Journal of Solid State Chemistry **145,** 619–628 (1999)
Article ID jssc.1999.8260, available online at http://www.idealibrary.com on IDEAL®

Electronic and Structural Effects of Nitrogen Doping on the Ionic Conductivity of γ-Li_3PO_4

Hassan Rabaâ* and Roald Hoffmann†,[1]

*Université Ibn Tofail, Laboratoire de Chimie Théorique Appliquée, Département de Chimie, P. O. Box 133, 14000 Kénitra, Morocco; and †Cornell University, Baker Laboratory, Department of Chemistry, Ithaca, New York 14853-1301, USA.

Received October 2, 1998; in revised form February 24, 1999; accepted March 10, 1999

Electronic and structural influences on ionic conductivity in the crystalline lithium phosphorus oxynitrides γ-Li_3PO_4 and $Li_{2.88}PO_{3.73}N_{0.14}$ are analyzed, using approximate molecular orbital calculations. Starting from γ-Li_3PO_4, we construct a model compound for the new nonstoichiometric oxynitride, $Li_{11}P_4O_{14}N$, in which an oxygen in a bridge position (O_{II}) in the parent γ-Li_3PO_4 structure is replaced by a nitrogen; in addition, oxygen and lithium defects are introduced in a systematic way. We examine the distortion of the lattice in response to substitution and defect formation. To study the P–N–P units observed in chromatographic studies of the oxynitride, density functional calculations are also carried out on small cluster models $[(HO)_3PNP(HO)_3)]^{1+}$, $[(HO)_3POP(HO)_3]^{2+}$, $[O(P_3(OH)_3)]^{4+}$, and $[N(P_3(OH)_3)]^{3+}$. To produce a high mobility of lithium species in the lattice, across tetrahedral faces rather than edges, our calculations suggest that a high concentration of defects is needed. © 1999 Academic Press

Key Words: **γ-Li_3PO_4; electronic structures; ionic conductivity.**

INTRODUCTION

Many phosphorus oxynitride electrolytes incorporate a remarkable amount of lithium and have been considered for possible application in rechargeable thin film lithium batteries (1). Nitrogen in the structure of amorphous lithium phosphate thin films (deposited by sputtering Li_3PO_4 in N_2) increases the lithium ion conductivity (2). Added nitrogen also increases the hardness of several phosphorus oxynitride glasses (3–6). The observed major improvement in chemical durability and other properties has been attributed to increased cross-linking between the chains of PO_4 tetrahedra. This results from the substitution of doubly (=N–) and triply (–N<) coordinated nitrogen for the bridging and nonbridging oxygen ions in the glass network (3). Recently, Wang *et al.* (5) have reported a neutron diffraction study of crystalline lithium phosphorus oxynitrides of γ-Li_3PO_4 [**A**] and the nitrogen-doped defect phase $Li_{2.88}PO_{3.73}N_{0.14}$ [**B**]. In this work we undertake an exploration of the electronic structure of these nitrogen-substituted lithium phosphates.

Let us first take a look at the crystal structure and the properties of γ-Li_3PO_4 [**A**]. Three polymorphs of Li_3PO_4 are known, stable at progressively higher temperatures: α, β, and γ-Li_3PO_4 (7–9).

β-Li_3PO_4 has a wurtzite superstructure: Li and P are in tetrahedral sites and all tetrahedra sharing vertices point in the same direction. With reference to the face-centred superlattice, all tetrahedral sites are occupied while the octahedral sites are unoccupied. On the other hand, in γ-Li_3PO_4 [**A**] (Fig. 1) some tetrahedra sharing vertices point in the opposite direction, similar to the arrangement of tetrahedral SiO_4 in the olivine structure (8). Each oxygen in β- or γ-Li_3PO_4 is shared by three LiO_4 tetrahedra (Fig. 1). The LiO_4 tetrahedra share vertices with PO_4 tetrahedra. A major difference between the β and γ structures is that some edge-sharing of LiO_4 occurs in γ-Li_3PO_4, whereas in β-Li_3PO_4 only vertex-sharing is present. Scheme 1 shows only a basic building block of the γ-Li_3PO_4 structure; for clarity we omit the PO_4 tetrahedra.

The crystal structure of γ-Li_3PO_4 [**A**] determined by neutron diffraction (5) reveals that the unit cell is orthorhombic, space group Pmnb with $Z = 4$. There are six atoms in the asymmetric unit: three tetrahedral cations (Li_I, Li_{II}, and P) and three oxygen anions (O_I, O_{II}, and O_{III}). Each $Li_{II}O_4$ tetrahedron shares adjacent edges with two Li_IO_4, which in turn share only corners with other Li_I tetrahedra (Scheme 1). There are twice as many tetrahedral Li_IO_4 units as $Li_{II}O_4$ units.

Let us consider the differences and similarities between the parent [**A**] and the nitrided [**B**] structures. In Table 1, we summarize the principal bond lengths and bond angles (5). One P–O distance in [**B**] is lengthened (from 1.54 to 1.58 Å) and another is shortened (from 1.54 to 1.49 Å). The

[1] To whom correspondence should be addressed. E-mail: rh34@cornell.edu. Fax: number: (607) 255-5707.

0022-4596/99 $30.00

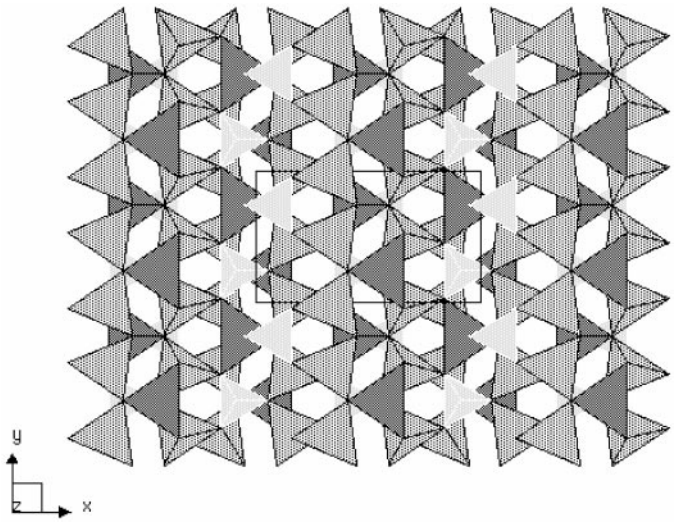

FIG. 1. Polyhedral crystal structure view alonmg (00) of γ-Li_3PO_4. The lighter shaded tetrahedra are PO_4. The Li_IO_4 and $Li_{II}O_4$ tetrahedra are further distingushed by dark and gray shading, respectively.

oxygen O_{II} and O_{III} positions are substantially perturbed upon incorporation of nitrogen into the lattice. Even the Li–O distances are affected, and the variation of O–Li–O bond angles is also significant. Despite all these changes, the unit cell volume of [**B**] remains nearly identical to that of [**A**]. A definitive decision on the placement of the nitrogen in structure [**B**] could not be reached from the experimental data.

What might one expect upon nitrogen incorporation in the lattice? Substitution of nitrogen for oxygen should lengthen some Li–O and P–O distances since the greater effective ionic radius of N^{3-} (1.32 Å) is greater than that of O^{2-} (1.24 Å) (9). The bond distance changes are related to tetrahedral distortion. When nitrogen is incorporated into the structure, both the P and the Li tetrahedra are distorted. The bond valence sums $V_i = \sum b_{ij}$ (V_i = valence of atom i, b_{ij} = bond valence between atom i and neighboring atom j) (5) of the oxygen site in [**A**] are all near the expected value (O_I, 1.97; O_{II}, 2.03; and O_{III}, 2.09, as computed using the bond valence parameters of Brown and Altermatt (10)). Incorporation of nitrogen in [**B**] produces some changes in the bond valence sum (O_I, 1.93; O_{II}, 2.23; and O_{III}, 1.88). It is this observation which leads us to say that O_{II} or O_{III} is strongly affected by the introduction of nitrogen.

Wang *et al.* (5, 6) also provide a chromatogram (HPLC) of $Li_{2.88}PO_{3.73}N_{0.14}$ [**B**] which contains features not found in the chromatogram of γ-Li_3PO_4 [**A**]: in particular, some peaks are identified as P–N–P fragments and other peaks as PO_3N. The P–N–P fragments are interesting, in that in γ-Li_3PO_4 all PO_4 tetrahedra are isolated from each other; i.e., there is no P–O–P linkage. To form the P–N–P units one must postulate some P exchange with Li in neighboring tetrahedra. The experimental observation of P–N–P fragments also indicates much difference between O and N in terms of their bonding to P ions.

The above-quoted study of ionic conductivities indicates that the incorporation of a small amount of nitrogen in the

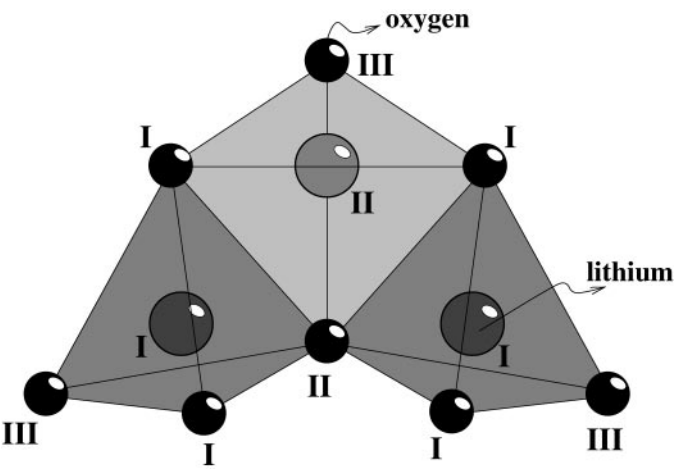

SCHEME 1. A partial structure of γ-Li_3PO_4, showing edge of two Li_IO_4 with one $Li_{II}O_4$. The dhading of tetrahedra is the same as in Fig. 1. The small circles are oxygen atoms, the big ones are lithiums. The light tetrahedron contains lithium (II) atoms and the dark tetrahedra lithium (I).

TABLE 1
Selected Interatomic Distances (Å) and Angles (°) for γ-Li_3PO_4 and $Li_{2.88}PO_{3.73}N_{0.14}$ from Ref. (5)

	γ-Li_3PO_4 [**A**]	$Li_{2.88}PO_{3.73}N_{0.14}$ [**B**]
PO_4 tetrahedron		
$P–O_I$	1.539	1.538
$P–O_I$	1.539	1.438
$P–O_{II}$	1.533	1.497
$P–O_{III}$	1.547	1.583
$O_I–P–O_I$	109.6	111.4
$O_I–P–O_{II}$	110.0	112.5
$O_I–P–O_{III}$	112.5	108.8
$LiIO_4$ tetrahedron		
$LiI–O_I$	1.951	2.001
$LiI–O_{II}$	1.936	1.886
$LiI–O_{III}$	1.913	1.936
$O_I–LiI–O_I$	106.2	105.1
$O_I–LiI–O_{II}$	96.2	101.2
$Li_{II}O_4$ tetrahedron		
$Li_{II}–O_I$	1.995	1.974
$Li_{II}–O_{II}$	2.043	2.106
$Li_{II}–O_{III}$	1.926	1.944
$O_I–Li_{II}–O_I$	128.5	129.5
$O_I–Li_{III}–O_{II}$	93.3	95.0

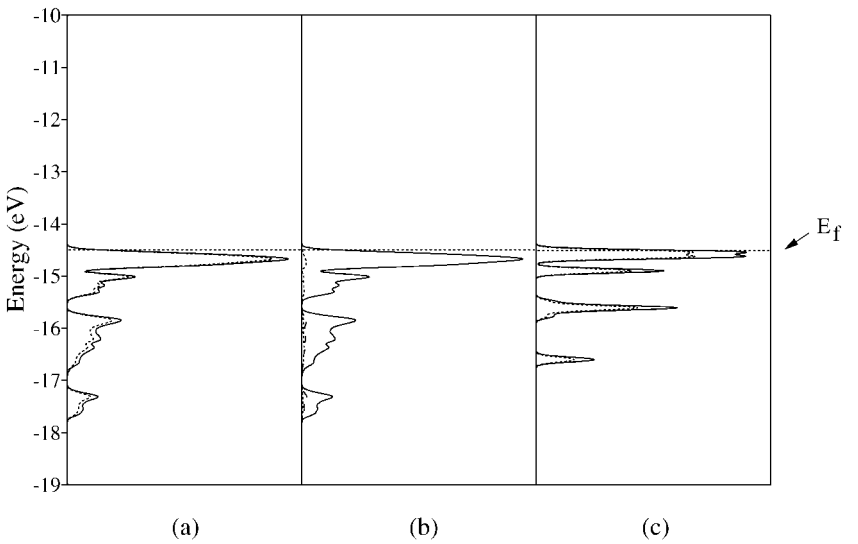

FIG. 2. (a and b) Total density of states of γ-$Li_{12}P_4O_{16}$ [**A**]; (c) the $PO_4)^{3-}$ sublattice of structure [**A**]. In each case the total DOS is the solid line. The contribution of the followings atoms are shown: (a) Oxygen atoms in [**A**], (b) phosphorus atoms in [**A**], (c) oxygen in the isolated $(PO_4)^{3-}$ sublattice of [**A**].

lattice increases the conductivity by a factor of about 40. As mentioned above, the neutron diffraction data does not indicate unambiguously which of the oxygen sites are occupied by nitrogen.

The purpose of this work is to analyze theoretically the structural and electronic effects of nitrogen substitution in γ-Li_3PO_4 by using the density of states (DOS) and crystal orbital overlap population (COOP) curves obtained from an approximate molecular orbital procedure for studying the electronic structure of extended materials, the extended Hückel method (11–14). Particular attention is given to the effect of nitrogen on the structure by constructing and analyzing a model similar to the nitrogen-doped [**B**]. In tandem with these extended structure calculations, to understand the existence of the P–N–P unit in [**B**], we compare the P–O–P and P–N–P linkages with model molecular calculations employing density functional theory (15–19). In the last section, we study a model for lithium ion mobility in the lattice and try to find relationships between structure and properties in these compounds.

γ-Li_3PO_4

Let us look first at the electronic structure of undoped γ-Li_3PO_4 [**A**]. Our investigations are based on the observed crystal structures of [**A**] and [**B**] (5). We begin with [**A**], for which we calculated the density of states of [**A**] and of just its $(PO_4)^{3-}$ sublattice (Fig. 2). In the DOS of the $(PO_4)^{3-}$ sublattice (Fig. 2c), the first peak, just below the Fermi level, corresponds to the band formed by oxygen lone pairs with little P admixture. Below this are two bands which are also mainly oxygen, but which (as we will see) have P–O bonding character. Near -35 eV, below the energy window of this figure, is the 2s(O) band.

Figures 2a and 2b show the O and P contributions to the DOS of γ-Li_3PO_4 structure. The Fermi level is near -14.5 eV. Note how the two lower bands are stabilized in the full structure relative to the isolated $(PO_4)^{3-}$ sublattice of Fig. 2c. This must be due to Li–O interaction. Lithium–oxygen interaction is also indicated by the fact that the three principal bands in the full structure are more dispersed than in the phosphate sublattice alone (compare Figs. 2a and 2c). The lithium contribution to the DOS shows only a slight admixture of Li states, actually surprisingly little given the stabilization in energy of the lower peaks. The average calculated net charge of lithium is $+0.65$, consistent with a substantially ionic formulation.

COOP (13) curves were also calculated for different P–O and Li–O bonds. The positive and negative regions in the COOP indicate bonding and antibonding interactions, respectively. Figure 3 shows strong bonding between P and O, concentrated in the two lower bands. This COOP also shows from -14.5 up to -17.8 eV a good bit of Li–O bonding. The P–O and Li–O average overlap populations are 0.64 and 0.15, respectively. The Li–O overlap population is clearly not negligible (11, 12) (see comments in Appendix on Li parameters).

We next calculated structure [**B**] as if it had no nitrogen and no defects. As one can see from Table 2, the three types of oxygen bear different charges (-1.13, -1.09, -1.17, respectively, for O_I, O_{II}, and O_{III}). Oxygen O_{II} is less negative than O_{III} and O_I because it is located in a bridge position, between three lithiums. There are good experimental and theoretical reasons for supposing that if substitution by

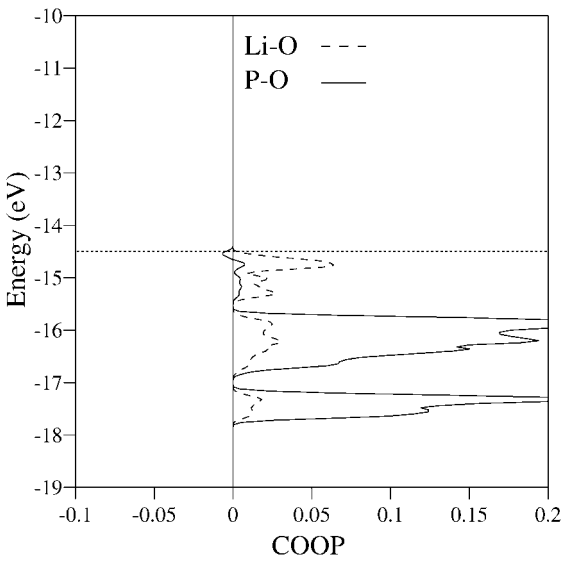

FIG. 3. P–O and Li–O COOP polts ofr $Li_{12}P_4O_{16}$ [**A**]. The average of all the different COOPS is plotted.

a less electronegative atom (nitrogen for oxygen) is desired, it would take place at the less negatively charged oxygen (20). This is O_{II}.

Defect creation and incorporation of nitrogen should lead to a modification of the electronic structure of the framework. In the following section, we first consider nitrogen substitution and defect creation by building a structural model for the nitrided defect phase.

CONSTRUCTING A MODEL FOR $Li_{2.88}PO_{3.73}N_{0.14}$

The real material we wish to study is nonstoichiometric $Li_{2.88}PO_{3.73}N_{0.14}$. However, for calculations with translational symmetry we need a stoichiometric model. No matter what model we choose, the unit cell will be quite large. For instance, starting with nitrogen doping, about a thousand alternative configurations are in principle possible: we have three types of oxygen to be substituted by N, and two types of lithium and the same oxygen variety to be removed.

Among these many possibilities, a reasonable model for $Li_{2.88}PO_{3.73}N_{0.14}$ can be found with some chemical and physical selection criteria, especially charge and valence considerations. For instance, as we argued above, the substitution of less negatively charged oxygen by nitrogen is obviously better. We begin from the idealized structure [**A**], after which we will move to the observed coordinates of [**B**].

The charge distribution argues for replacement of the most positive O_{II} by N. Starting from structure [**A**], our calculations show a relative stabilization energy about 0.2 eV when we substitute O_{II} (instead of O_{III} or O_I) by N. This agrees with the variation of bond distances from X-ray data (see Table 1), which points to substitution of O_{II} and/or O_{III} by nitrogen. This substitution leads to the first model compound $(Li_{12}P_4O_{15}N)^{-1}$; this is derived from $Li_{12}P_4O_{16}$ by substituting one O_{II}^{2-} by an N^{3-} ([**C**] in Scheme 2).

In creating a model for a lithium vacancy, we are guided by the Pauling rules (21) for an ionic solid. The first rule we apply is to minimize cation–cation repulsion. The Li_{II} atom in the $Li_{II}O_4$ tetrahedron would be the most probable site for defect formation, for it is surrounded by two lithium cations. By creating the defect there we reduce cation–cation repulsions and obtain the next stage of a model, $(Li_{11}P_4O_{15}N)^{2-}$ ([**D**] in Scheme 2).

Next we want to remove one oxide ion from [**D**] to obtain a neutral $Li_{11}P_4O_{14}N$ [**E**]. Our calculations indicate that O_{III} is the best candidate to be removed (we find a net stabilization energy of about 0.3 eV upon removing O_{III} vs O_{II} or O_I). Thus a concentration of lithium defects near the incoming nitrogen and near an oxygen that is removed seems electronically more promising. This substitution pattern is consistent with the structural data and explains in particular the long and short $P–O_{II}$ and $P–O_{III}$ distances seen previously in Table 2. The model we have, $Li_{11}P_4O_{14}N$, ([**E**] in Scheme 2) is equivalent to $Li_{2.75}PO_{3.50}N_{0.25}$. This is close in stoichiometry to the real formula, $Li_{2.88}PO_{3.73}N_{0.14}$ [**B**].

A DOS plot for [**E**] is shown in Fig. 4a, with the contribution of O indicated by dotted regions. Note that the energy window is smaller here than in the other figures shown. In Figs. 4b and 4c the contributions of N and P, respectively, are indicated. We first note that the Fermi level moves up slightly to -13.5 eV. The narrow band at -13.5 eV is actually filled, the placement of the Fermi level in what seems to be the middle of a band just an artifact of the smoothing of the densities in the computations (22). In Fig. 4b (in the energy range between -11.5 and -14.3 eV) we

TABLE 2
Average Atomic Net Charges and Overlap Populations Computed for γ-Li_3PO_4 [A] and [B][a]

	γ-Li_3PO_4 [**A**]	$Li_{12}P_4O_{16}$[**B**]
Net charges		
P	2.632	2.630
Li_I	0.629	0.628
Li_{II}	0.649	0.642
O_I	−1.135	−1.130
O_{II}	−1.131	−1.094
O_{III}	−1.138	−1.172
Overlap populations		
P–O	0.643	0.643
Li–O	0.150	0.140
$P–O_{II}$	0.712	0.765

[a] The calculations were performed for the geometry of [**B**] without nitogen substitution and defects.

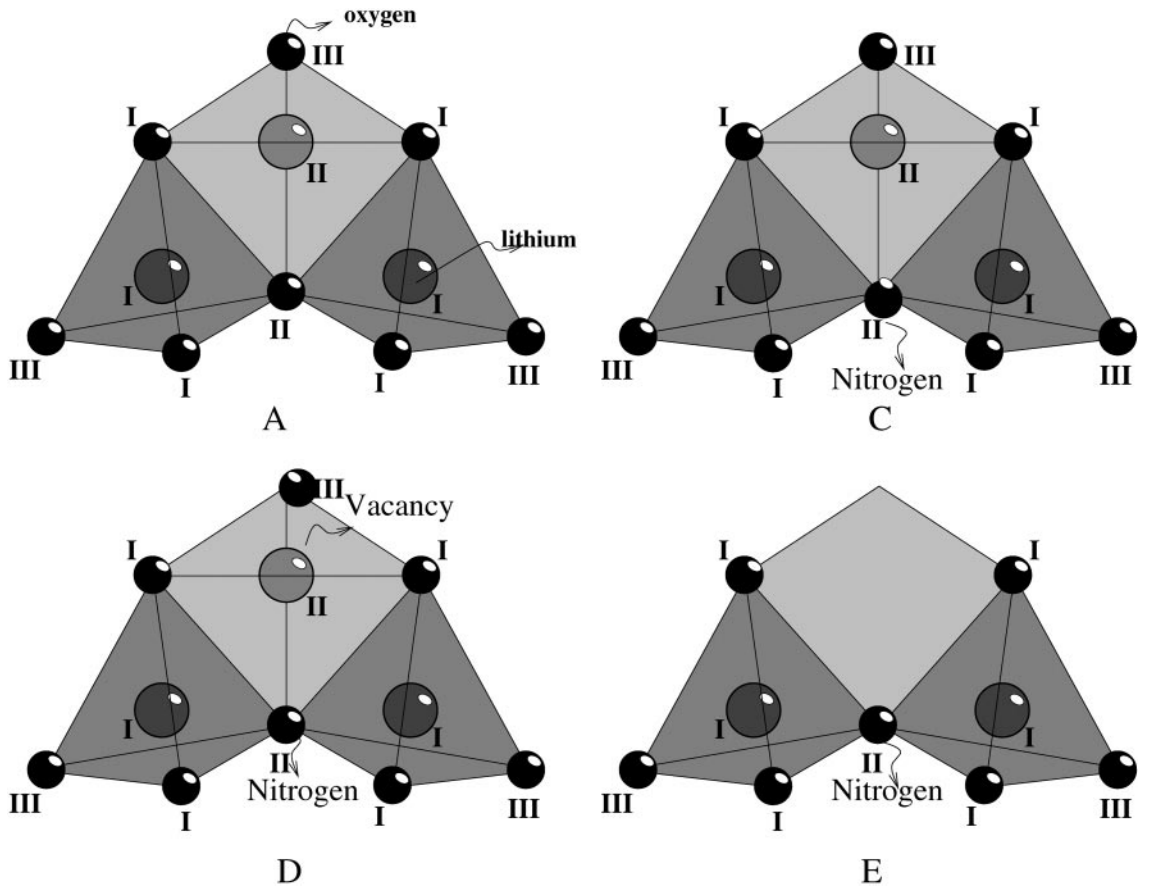

SCHEME 2. Steps in the construction of the model. [**A**] The starting point, all atoms in the the block retained; [**C**] nitrogen substituted in the O_{II} position; [**D**] a vacancy created in the Li_{II} position; [**E**] oxygen is removed from the O_{III} position.

observe that N dominates the DOS contributions. The introduction of nitrogen gives three narrow peaks near the Fermi level. On comparing Figs. 2 and 4, we note that the higher energy part of the valence band is characterized by the O_{2p} nonbonding levels in [**A**] and N_{2p} in [**E**]. From Figs. 4 and 5, we see that some of the unfilled antibonding

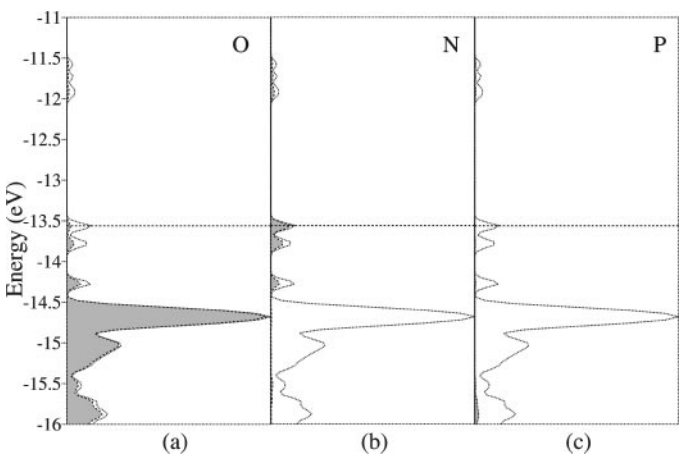

FIG. 4. Total density of states of $Li_{11}P_4O_{14}N$ [**E**]. In each case the total DOS is the solid line. The contributions of the followings atoms are shown (shaded areas): (a) oxygen atoms, (b) nitrogen atoms, (c) phosphorus atoms.

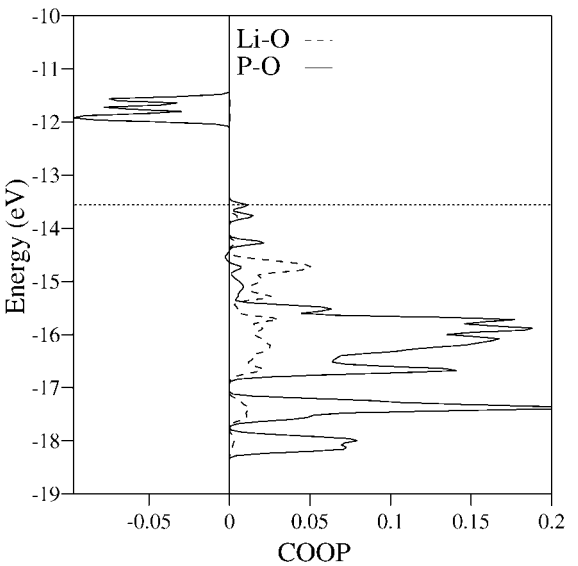

FIG. 5. An average of P–O and Li–O COOP plots for $Li_{11}P_4O_{14}N$ [**E**].

P–O bands drop in energy (they are at around -12 eV in [**E**] vs. -6 eV in [**A**]), pointing indirectly to a weakening of the P–O bonds (23). The P–N overlap population in [**E**] is 1.10, indicating significant P–N bonding.

Models [**C**]–[**E**] were based on the γ-Li_3PO_4 structure [**A**]. We next took the observed nitrided defect structure $Li_{2.88}PO_{3.73}N_{0.14}$ [**B**] and built (following exactly the same reasoning as for [**A**]) a stoichiometric model based on that geometry. This is [**F**]. The DOS and the COOP of the new $Li_{11}P_4O_{14}N$ model [**F**] is shown in Figs. 6 and 7, respectively. The similarities between the DOS and the COOP of [**E**] and [**F**] (Figs. 4–7) are evident. However, the net charges in [**F**] are slightly decreased for each atom (see Table 3). The average overlap populations (OP) computed for P–O and Li–O bonds are almost the same in [**E**] and [**F**]. There is a significant difference between the P–N OPs in [**E**] and [**F**] as a consequence of the bond length differences in underlying models [**A**] and [**B**] (see Table 1). The distortion of the tetrahedra is more pronounced in [**F**] and could be responsible for the small shift in some of the peaks in the DOS (for instance, the peak at -11.5 eV in Fig. 4 has moved to -11.1 eV in Fig. 6). The COOP curve of [**F**] is not really different from that of [**E**]. It appears that either of the models constructed, [**E**] or [**F**], represents adequately $Li_{2.88}PO_{3.73}N_{0.14}$.

The new P–N bond probably adds some bonding and stability to this material (3), and is responsible for the observed distortions. The deformation from regular PO_4 to irregular PO_3N tetrahedra and from LiO_4 to LiO_3N in [**E**] will change the charge and the environment of the central Li or P atoms.

It is obvious that if we break some P–O or Li–O bonding in the parent [**A**] (by substitution and vacancy formation), the Li–O and P–O interactions will change and lead to some difference in the shape of the DOS. We probed this point with a calculation on a hypothetical $(PO_3N)^{4-}$ sublattice, shown in Fig. 8b, with the contribution of N indicated by shaded regions in Fig. 8c. For comparison of $(PO_4)^{3-}$ and $(PO_3N)^{4-}$ sublattices, we reproduce in Fig. 8a the $(PO_4)^{3-}$ DOS. The total band width of the $(PO_3N)^{4-}$ sublattice is greater than in $(PO_4)^{3-}$ (compare Figs. 8a and 8b), if we include the mainly N higher bands. We note also that the two lower bands are more dispersed in the $(PO_3N)^{4-}$ sublattice (Fig. 8b) relative to the isolated $(PO_4)^{3-}$ sublattice of Fig. 8a. This must be due to P–N interaction.

Next, let's see what happens upon P–N–P bonding.

THE P–N–P BOND LINKAGE

To form the P–N–P units one must postulate some exchange of P with Li in neighboring tetrahedra. Let's look at two vertex-sharing tetrahedra of Li and substitute one lithium with phosphorus (Scheme 3). The radii of P^{4+}(0.6 Å) and Li^+(0.5 Å) as one might think (9). The two tetrahedra can be modeled by $[(O_3)PNLi(O_3)]^q$. LDA calculations (16–19) were carried out on four simple cluster models: $[(HO)_3POP(HO)_3]^{+2}$ [**G**], $[(HO)_3)PNP(HO)_3)]^{+1}$ [**H**], $[O(P(OH)_3)_3]^{4+}$ [**I**], and $[N(P(OH)_3)_3]^{+3}$ [**J**] (Scheme 4). In cutting the cluster out of the lattice, we passivated the oxygens with hydrogen (see also the Appendix for computational details of the LDA method).

We show in Scheme 4 two models, $[(HO)_3POP(HO)_3]^{+2}$ [**G**] and $[(HO)_3)PNP(HO)_3)]^{+1}$ [**H**], whose structures were optimized with the results shown in Table 4. We observe that the P–N–P and P–O–P angles are still close to

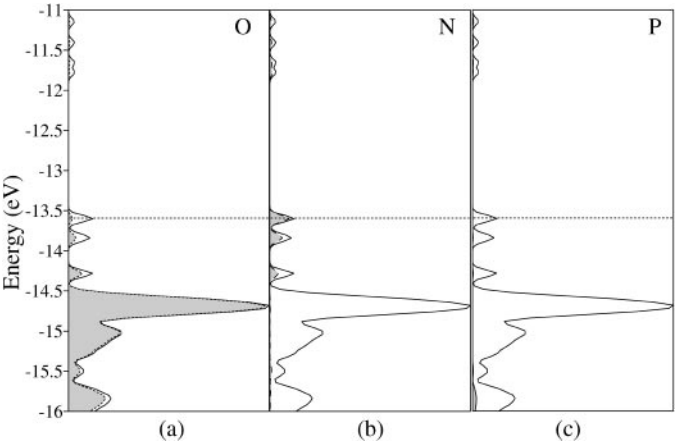

FIG. 6. DOS plot of $Li_{11}P_4O_{14}N$ [**F**]. The shaded regions correspond to the contributions of: (a) oxygen atoms, (b) lithium atoms, (c) phosphorus atoms.

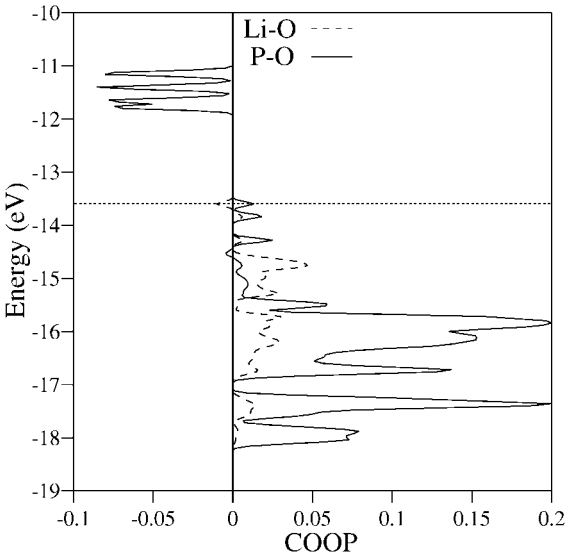

FIG. 7. An average of P–O and Li–O COOP plots for $Li_{11}P_4O_{14}N$ [**F**].

180°, indicating a linear geometry for [**G**] and [**H**]. One can explain this near linearity in terms of π conjugation involving the $P(OH)_3$ moiety. The heteroatom (X = O or N) lone pair orbital is substantially stabilized by mixing with the σ^* acceptor orbitals of the $P(OH)_3$, a mixing that is optimized in linear geometry.

In Table 4, the computed P–N bond distance (1.53 Å in [**H**]) is shorter than a P–N single bond (1.70 Å) or even a P=N double bond (1.60 Å), as judged from the literature (24). In both cases [**G**] and [**H**] the P–O distance is near that of a single bond. We observe also that the ($X–P–O_t$) bond angle is larger in [**H**]. This corroborates what we have seen happen in the crystal structure when we introduce nitrogen into the lattice (Table 1): some angle opening (for example for $O_I–P–O_{II}$) and some bond length shortening, such as 1.50 Å for $P–O_{II}$. However, we also note an elongation of other bonds, e.g., $P–O_{III}$.

The net charges obtained after interaction from our LDA calculation for phosphorus in [**G**] and [**H**] are +1.21 and +0.84, respectively. The net charge on the bridging oxygen in [**G**] is −0.17 and for N in [**H**] is −0.23.

Recently SCF-MO *ab intio* calculations were reported for $[(HO)_3PO_bP(HO)_3]^{+2}$ [**G**] (25, 26). The authors optimized the $P–O_b–P$ bond angle; the P–O–P linkage is bent near 160°. A similar angle is observed in a disiloxyether, such as $[(OH)_3SiOSi(OH)_3]$ (27–29). The Si–O–Si linkage is bent, and the Si–O bond length decreases as the Si-O-Si bond angle approaches 180°. The latter effect has been explained in terms of interaction of the oxygen lone pair orbitals with π-type acceptor orbitals of the SiO_4 groups. Presumably a similar effect is operative for the PO_4 grouping (30).

We have also carried out LDA calculation on two other clusters: $[O_b(P(OH)_3)_3]^{4+}$ [**I**] and $[N_b(P(OH)_3)_3]^{+3}$ [**J**]

TABLE 3
Average Atomic Net Charges and Overlap Populations for [E] and [F][a]

	γ-$Li_{11}PO_4O_{14}N$	$Li_{11}P_4O_{14}N$
Net charges		
P	2.10	2.10
Li	0.63	0.60
O	−1.13	−1.05
N	−1.04	−1.04
Overlap populations		
P–O	0.621	0.622
Li–O	0.140	0.130
P–N	1.091	1.158
Li–N	0.160	0.180

[a] Models [**E**] and [**F**] are based upon the X-ray structures of [**A**] and **B**], respectively.

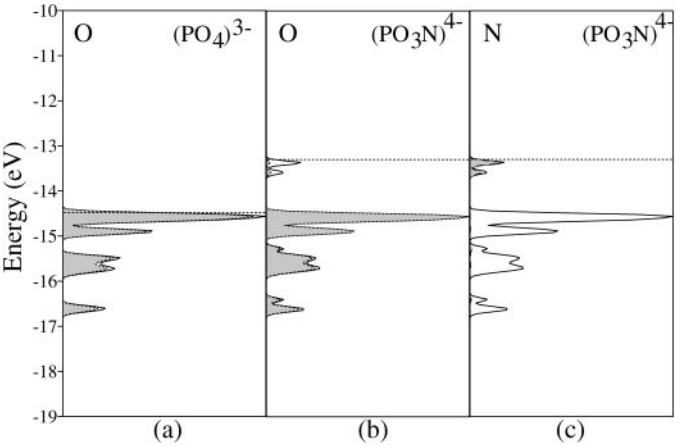

FIG. 8. Total density of states of hypothetical $(PO_3N)^{4-}$ and $(PO_4)^{3-}$ sublattices (solid line). The contribution of the followings atoms is shown (shaded area): (a) oxygen atoms in $(PO_4)^{3-}$, (b and c) oxygen and nitrogen atoms, respectively, in $(PO_3N)^{4-}$.

(Scheme 4). In these we find long $P–X_b$ distances (1.87 Å in [**I**] compared to 1.72 Å in [**J**]). In [**J**] the XPO_t angle is larger than in [**I**], by 5°. Both of these two geometries are planar (at O_b or N_b), the planarity presumably arising from hyperconjugation of the lone pair on the central N or O with $P(OH)_3$ σ^* orbitals. But the optimized molecular parameters are still different (see Table 4). We observe that [**I**] and [**J**] have the same tendency as seen before for [**G**] and [**H**]: the bond angle ($N–P–O_t$) is increased and the P–O bond is lengthened.

We find in [**H**] and [**G**] a short P–N distance. This also may be related to the magnitude of electron transfer from the higher energy lone pair of nitrogen or oxygen to σ^* acceptor orbitals of $P(OH)_3$, which should be more important for N than for O.

In conclusion, nitrogen incorporation really affects the geometries of these small model clusters, both bond lengths and bond angles. It leads to some distortion. The reasonable energies and geometries of our model systems imply that the formation of the P–N–P unit is plausible, but we have not studied this substitution, nor any associated relaxation, in extended systems.

IONIC CONDUCTIVITY

Let us consider the effect of nitridation on the ionic transport in these materials (23, 30). The interaction between the interstitial Li^+ ions and each oxide and the four network cations to which the oxide is bonded is related to the size of the bottleneck (tight passage) between interstitial sites. The diminished size of the bottleneck in [**A**] probably accounts for the relatively high activation energy reported in (5), thus leading to the small Li mobility in the lattice. In

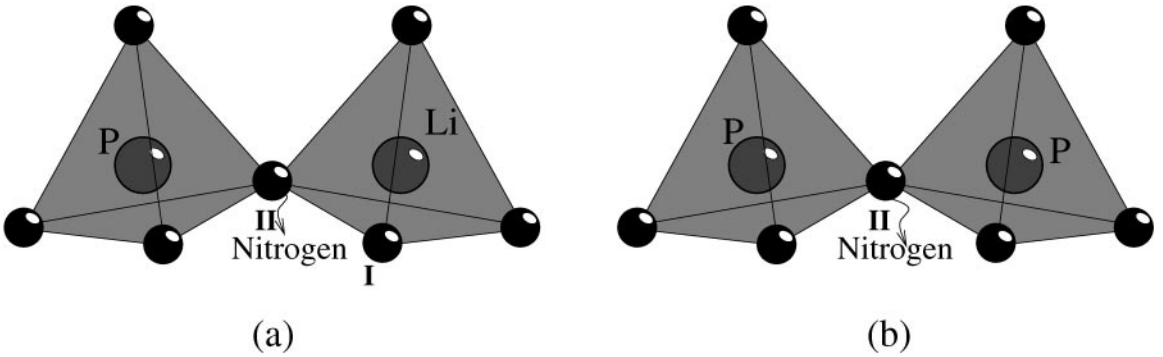

SCHEME 3. (a) Taking two corner sharing tetrahedra of Li and P as $[O_3]PNLi(O_3)]^q$ units; (b) substituting one lithium by phosphorus.

the structure of [**A**], a Li^+ in the middle of a face of a tetrahedron would be 2.08 Å from the oxygens, but at the midpoint of an edge it would be 1.12 Å. It is clear that the Li ions will have less difficulty in crossing the face rather than the edge of LiO_4 tetrahedra.

In the conduction process, the Li ions need to move further in the lattice. As we saw in the previous section, by substituting N for O and creating a concentration of Li defects, the O–P–O and O–Li–O angles were increased in [**B**] compared to that seen in [**A**]. If we compare [**A**] and [**B**], the main difference found in our calculation was the distortion of tetrahedra due to nitrogen incorporation (i.e., PO_3N) and the creation of oxygen defects. This distortion should also improve substantially the free space in the lattice, allowing Li^+ to move more easily.

Experimentally, we know from the ionic conductivity data for [**B**] that the incorporation of a small amount of nitrogen in the lattice increases the conductivity by a factor of about 40 (5). We would like to understand this facilitation of Li^+ movement.

In Scheme 5 we show three edge-sharing tetrahedra of Li taken from the crystal structure of [**A**], two of which share vertices with PO_4 tetrahedra. There is an unoccupied, approximately octahedral site in the center of these four tetrahedra. This octahedral site (marked by a lined circle in Scheme 5) is surrounded by six neighboring oxygen atoms (O1–O6). The presence of such a vacant site should facilitate the jumping of Li atoms between various Li positions in the

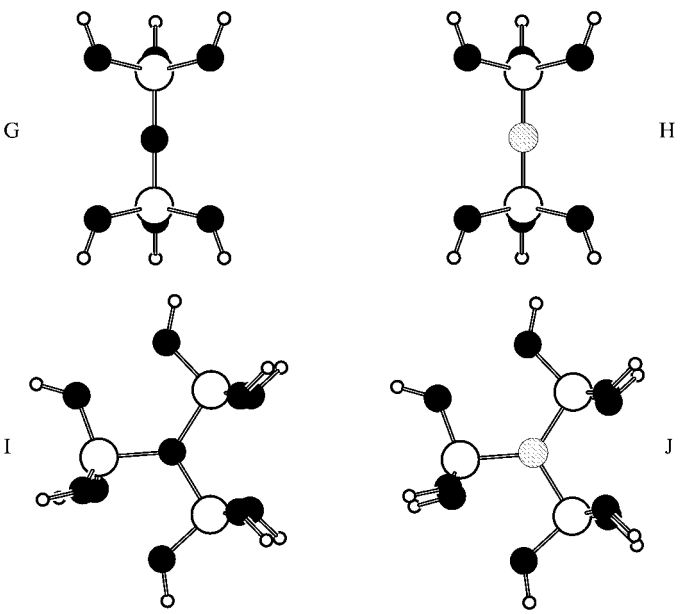

SCHEME 4. DFT calculated minimum structures of $[(HO)_3POP(HO)_3]^{+2}$ [**G**], $[(HO)_3)PNP(HO)_3)]^{+1}$ [**H**], $[O(P(OH)_3)_3)^{4+}$ [**I**], $[N(P(OH)_3)_3^{+3}$ [**J**]. The dark small circles are oxygen atoms, the dark big circles are phosphorus atoms and the light circles are hydrogen atoms. In [**H**] and in [**J**] the bridging atom (shaded circle) is nitrogen.

TABLE 4
The Optimized Geometries and Atomic Net Charges of $[(OH)_3PXP(OH)_3)]^q$ (X = O, N) and $[((OH)_3P)_3X]$

	[**G**]	[**H**]	[**I**]	[**J**]
Distances and bond angles				
P–X	1.575	1.538	1.875	1.719
P–O	1.551	1.587	1.525	1.542
O–H	0.987	0.979	1.004	0.991
P–X–P	179.0	179.9	119.7	119.6
X–P–O_t[a]	101.4	108.1	100.5	105.1
O–P–O	116.0	110.1	118.9	115.5
Net charges				
P	1.21	0.84	1.34	1.14
X	−0.17	−0.23	−0.43	0.02
O	−0.33	−0.41	−0.26	−0.30

Note. Distances are in Å and angles are in degrees.
[a] O_t, terminal oxygen.

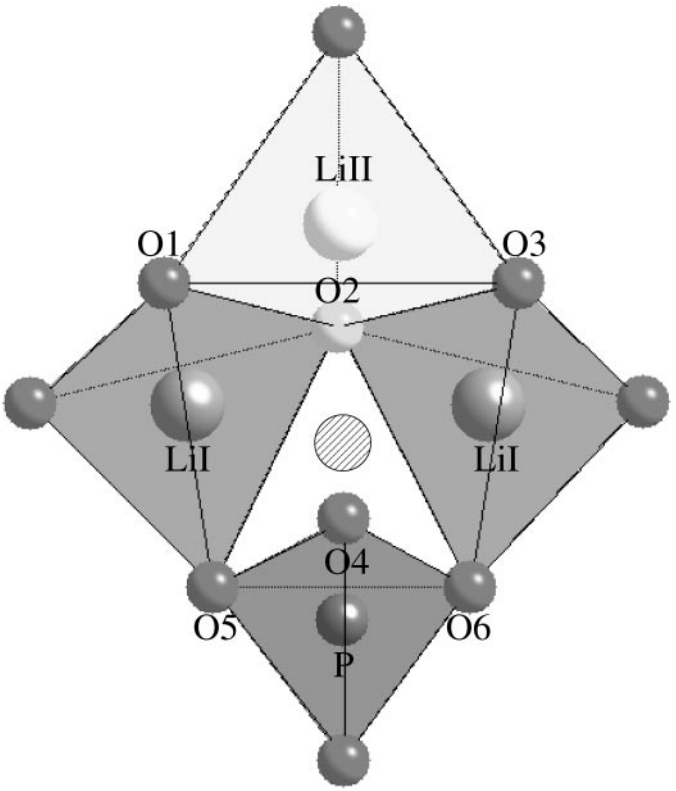

SCHEME 5. A set of three adjacent LiO_4 tetrahedra, two of which (Li_I) share vertices with PO_4 tetrahedra in the γ-Li_3PO_4 structure. The dark circles are oxygen atoms; the light circles are lithium atoms. The lined circle makes the center of the unoccupied octahedral site surrounded by the six oxygen atoms, O1–O6.

original crystal structure. The energy of the octahedral site is lower by 0.25 eV than that of the tetrahedral site in [**B**] compared to [**A**]. This octahedral site exists in [**A**] and in [**B**]. However, as mentioned before, with nitrogen substitution and Li and O defects in [**B**], these cavities (octahedral sites) are larger in [**B**] than in [**A**], leading to greater mobility of Li^+ (5).

The above reasoning argues for an easier Li^+ jump between these sites in [**B**], but what about the energy barrier to Li^+ motion? In Scheme 6, we show three edge-sharing tetrahedra of Li taken from the crystal structure of [**A**]; Li_{II} is removed as was indicated in Scheme 2. One possible pathway for Li^+ motion is across the shared faces of LiO_4 tetrahedra. We add in Scheme 6 two virtual dummy atoms marking the intermediate position of the ions if they were to move across the shared faces of Li_IO_4 and $Li_{II}O_4$ tetrahedra. Regretably, we cannot calculate reliably the actual barrier to motion between the two sites with our method. In the future we will use another computational procedure (32) to evaluate the pathways of lithium ion motion in the network. Then we can connect the activation energy to the ionic conductivity.

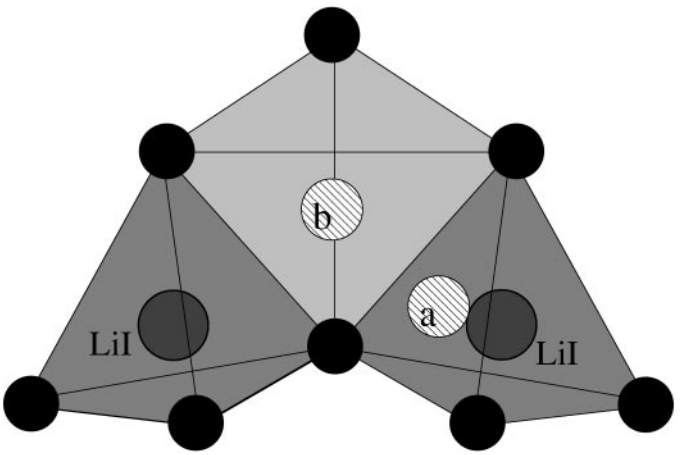

SCHEME 6. A model for lithium mobility across shared tetrahedral faces in [**B**]. Two dummy atoms (shaded areas) indicate the assumed intermediate positions of Li atoms: (a) corresponding to crossing the center of a Li_IO_4 face and (b) corresponding to crossing the center of $Li_{II}O_4$ face.

CONCLUSION

Electronic structure calculations were performed on both γ-Li_3PO_4 [**A**] and $Li_{2.88}PO_{3.73}N_{0.14}$ [**B**]. By using a simple model and considering different structural possibilities, we found that a concentration of lithium defects near the incoming nitrogen (and near an oxygen that is removed) is favored. A distortion of LiO_4 and PO_4 tetrahedra in [**B**] is also indicated.

LDA calculations indicate that a Li/P disorder and the formation of P–N–P units in the lattice is plausible. The geometry of our model clusters was really affected by the incorporation of nitrogen.

Li mobility in these structures should be related to the creation of defects and distortion of tetrahedra. That mobility is higher in [**B**] than in [**A**]. The energy difference between possible Li^+ positions, related to the cation jump between a tetrahedral and octahedral sites, is calculated.

ACKNOWLEDGMENTS

The work at Cornell was supported by the National Science Foundation through Research Grant CHE 94-08455. H.R. thanks the Hoffmann research group at Cornell University for useful comments and suggestions and Dr. D-K. Seo for helpful discussions. H.R. is grateful to the Foreign Ministry of the Kingdom of Morocco for their contribution to his travel.

APPENDIX

1. Extended Hückel calculations. The program YAeHMOP (Yet Another extended Hückel Molecular Orbital Package) (14), an extended Hückel implementation of the tight binding method, was used in all extended system calculations. Table 5 lists the parameters for the elements

TABLE 5
Parameters Used in the Extended Hückel Calculations (11, 12)

Atom	Orbital	H_{ii}(eV)	ξ
Li	2*s*	−9.0	0.703
	2*p*	−8.0	0.703
P	3*s*	−18.6	1.75
	3*p*	−14.0	1.30
N	2*s*	−26.0	1.950
	2*p*	−13.4	1.950
O	2*s*	−32.3	2.275
	2*p*	−14.8	2.275

that are used in this work (11–14). A 64 k-point set was used for all structures (15). The Li–O overlap population was very small when a "molecular" set of H_{ii} parameters of lithium is used. This led us to employ another set of H_{ii} parameters (a so-called "solid" set) for Li.

2. Density functional calculations. The electronic structure calculations on the small cluster models were carried out using the ADF program (16–18). The ground state structures of $[(HO)_3POP(HO)_3)]^{2+}$, $[(HO)_3PNP(HO)_3]^{1+}$, $([O(P(OH)_3)_3]^{4+}$, and $[N(P(OH)_3)_3]^{3+}$ units were determined by means of the standard optimization algorithm (18). The local density approximation (LDA, VWN) was used (33). For all calculations the TZVP basis set type IV was used (19).

REFERENCES

1. J. B. Bates, G. R. Gruzalski, N. J. Dudney, C. F. Luck, X-H. Yu, and S. D. Jones, *Solid State Technol.* **59** (1995).
2. J. B. Bates, G. R. Gruzalski, N. J. Dudney, R. A. Zuhr, A. Choudhury, C. F. Luck, and J. D. Robertson, *Solid State Ionics.* **53,** 647 (1992).
3. A. Le Sauze, R. Marchand, and E. Gueguen, *J. Non-Cryst. Solids* **217,** 83 (1997).
4. M. R. Reidmeyer and D. E. Day, *J. Non-Cryst. Solids* **181,** 201 (1995); *J. Non-Cryst. Solids* **177,** 208 (1994).
5. B. Wang, B. C. Chakoumakos, B. C. Sales, B. S. Kwak, and J. B. Bates, *J. Solid State Chem.* **115,** 313 (1995).
6. B. Wang, B. C. Sales, B. S. Kwak, and J. B. Bates, *J. Non-Cryst. Solids* **183,** 297 (1995).
7. E. Reculeau, A. Elfakir, and M. Quarton, *J. Solid State Chem.* **79,** 205 (1989).
8. Von J. Zemann, *Acta Crystallogr.* **13,** 863 (1960).
9. R. D. Shannon, *Acta Crystallogr. Sect. A.* **32,** 751 (1976).
10. I. D. Brown and D. Altermatt, *Acta Crystallogr. Sect. B* **24,** 244 (1985).
11. R. Hoffmann and W. N. Lipscomb, *J. Chem. Phys.* **36,** 2179 (1962).
12. R. Hoffmann, *J. Chem. Phys.* **39,** 1397 (1963).
13. R. Hoffmann, "Solids and Surfaces: A Chemist's View of Bonding in Extended Structures." VCH, New York, 1988.
14. G. A. Landrum, "Yet Another extended Hückel Molecular Orbital Package" (YAeHMOP), Cornell Univ. Press, New York, 1997; http://overlap.chem.cornell.edu:8080 /Yaehmop.html. (1995).
15. R. Ramirez and M. C. Böhm, *Int. J. Quantum Chem.* **30,** 391 (1986); *Int. J. Quantum Chem.* **34,** 571 (1988).
16. R. G. Parr and W. Yang, "Density-Functional Theory of Atoms and Molecules." Oxford Univ. Press, New York, 1989.
17. P. Hohenberg and W. W. Kohn, *Phys. Rev. B* **136,** 864 (1964).
18. R. M. Dreizler and E. K. U. Gross, "Density-Functional Theory." Springer-Verlag, New York, 1990.
19. A. D. Becke, *Phys. Rev. A* **38,** 3098 (1988); J. R. Perdew, *Phys. Rev. B* **33,** 8822 (1986), and references therein.
20. See for example: B. M. Gimarc, *J. Am. Chem. Soc.* **105,** 1979 (1983); J. K. Burdett, *Acc. Chem. Res.* **15,** 34 (1982).
21. L. Pauling, "The Nature of the Chemical Bond." Cornell Univ. Press, New York, 1960.
22. The densities of states were calculated in this paper every 0.02 eV and fit with Gaussians (exponent $-300(\Delta E)^2$) to obtain smooth curves. The result is a small broadening at the edges of each band, especially marked in this narrow band case.
23. G. Nuspl, K. Yoshizawa, and T. Yamabe, *J. Mater. Chem.* **7,** 2529 (1997).
24. For P–N–P, see for example: H. G. Heal, "The Inorganic Chemistry of Sulfur, Nitrogen, and Phosphorus." Academic Press, New York, 1980; A. F. Wills, "Structural Inorganic Chemistry," p. 660. Oxford Univ. Press, London, 1962.
25. D-K. Seo and M-H. Whangbo, *J. Solid State Chem.* **129,** 160 (1997).
26. N. S. Mandel, *Acta Crystallogr. Sect. B* **31,** 1730 (1975).
27. T. A. Albright, J. K. Burdett, and M-H. Whangbo, "Orbital Interactions in Chemistry," p. 149. Wiley and Sons, New York, 1985.
28. S. Sakka, *J. Non-Cryst. Solids* **181,** 215 (1995).
29. M. D. Newton, *in* "Structure and Bonding in Crystals" (M. O"Keefe and A. Navrotsky, Eds.), Vol. 1, Chap. 8. Academic Press, New York, 1981.
30. T. Okura, N. Aoki, and T. Kanazawa, *J. Non-Cryst. Solids* **95/96,** 427 1987
31. H. Y-P. Hong, *Mater. Res. Bull.* **13,** 117 (1978).
32. Work in progress.
33. S. Vosko, L. Wilk, and M. Nusair, *Can. J. Phys.* **2,** 41 (1973).